Nonstandard electroconvection with Hopf bifurcation in a nematic liquid crystal with negative electric anisotropies

Tibor Tóth-Katona, Aude Cauquil-Vergnes,* Nándor Éber, and Ágnes Buka
Research Institute for Solid State Physics and Optics, Hungarian Academy of Sciences, P.O.Box 49, H-1525 Budapest, Hungary
(Received 15 December 2006; published 20 June 2007)

Electric-field-driven pattern formation has been investigated in a nematic liquid crystal with negative dielectric and conductivity anisotropies. Despite the fact that the standard Carr-Helfrich theory predicts no hydrodynamic instability for such compound, experiments reveal convection patterns which we call nonstandard electroconvection (ns-EC). In this work, we characterize the ns-EC patterns by measuring the frequency, thickness, and temperature dependence of the threshold voltage, wave number, roll orientation, etc., and compare them with the standard-EC (s-EC) characteristics. For the first time, we report traveling rolls in ns-EC, and we give the dependence of the Hopf frequency on the driving frequency, temperature, and sample thickness. Finally, we discuss possible sources for the existence of these patterns.

DOI: 10.1103/PhysRevE.75.066210 PACS number(s): 47.54.−r, 61.30.Gd, 47.20.Lz

I. INTRODUCTION

Anisotropic fluids–liquid crystals (LCs)—are ideal materials for studying nonlinear, pattern forming phenomena in complex, nonequilibrium systems. Nematic LCs, the most common representatives of such substances, are uniaxial media whose easy direction is defined by the mean orientation of their rodlike molecules, the director **n**. Their material parameters are direction dependent, and one can define an anisotropy of the electrical conductivity $\sigma_a=\sigma_\parallel-\sigma_\perp$ or that of the dielectric permittivity $\epsilon_a=\epsilon_\parallel-\epsilon_\perp$ as the difference of values measured parallel ($\sigma_\parallel$, $\epsilon_\parallel$) and perpendicular ($\sigma_\perp$, $\epsilon_\perp$) to **n**, respectively [1].

Electroconvection (EC) in a thin layer of a nematic LC is a well-known example of electric field induced pattern forming instabilities [2,3]. It is most commonly observed in planarly aligned thin layers of nematic LCs with $\epsilon_a<0$ and $\sigma_a>0$. The initially homogeneous state becomes unstable when the applied ac rms voltage U of frequency f exceeds a threshold value U_c and a spatially periodic pattern (a set of rolls) characterized by a wave vector $\mathbf{q}_c$ develops. The pattern involves a distortion of the director field accompanied with vortex flow and charge separation. Theoretical explanation of the occurrence of EC patterns is based on the *Carr-Helfrich* mechanism, a one-dimensional (1D) model expressing the interplay between director tilt, space charges, and flow assuming an Ohmic electrical conductivity of the LC. This has later been extended to a complete three-dimensional description known as the standard model (SM) of EC [2,4]. The SM is able to deliver the frequency dependence of the threshold voltage $U_c(f)$ and the critical wave vector $\mathbf{q_c}(f)$, the director $\mathbf{n}(\mathbf{r})$, and the velocity $\mathbf{v}(\mathbf{r})$ fields, and the charge distribution $\rho_{el}(\mathbf{r})$ at onset, as well as some of the nonlinear (above threshold) features. It follows that depending on whether the frequency is below or above the so-called cutoff frequency f_c (related to the charge relaxation time), two types of stationary patterns may exist; in one type only the charge distribution oscillates with the applied ac voltage (conductive regime, low f) while in the other, on the contrary, the director and the flow follows the electric field (dielectric regime, high f). Though the patterns in the two regimes have significantly different $U_c(f)$ and $\mathbf{q}_c(f)$ characteristics, the refractive index modulation inherent in this deformation leads to a shadowgraph image (spatially periodic intensity variation via light focusing or defocusing effects [5]) when viewed in a microscope without or with a single polarizer, in addition to the birefringence image seen at crossed polarizers. Concerning the pattern morphology one can distinguish between rolls oriented perpendicular to the initial director (normal rolls, NR) or tilted ones where $\mathbf{q}_c$ includes an angle with **n** (oblique rolls, OR). The roll direction can be tuned continuously by varying the frequency. The OR to NR transition occurs at the Lifshitz point f_L. Various theoretical predictions of the SM have been compared with EC measurements on a number of nematics and usually a very good agreement has been obtained—see, e.g., [2,6,7].

Though the SM predicts a bifurcation to stationary EC patterns, occasionally (for some combination of f and $\sigma_\perp$) traveling waves (TWs) have been observed experimentally at threshold in various nematic LCs [8–11] indicating a Hopf bifurcation. In order to explain these features the assumption on Ohmic conductivity had to be given up in favor of a more realistic one: conductivity via oppositely charged ions. The theoretical extension of the SM by taking into account diffusion, recombination and dissociation of charge carriers is known as the weak electrolyte model (WEM) [12]. The inclusion of physical processes with extra time scales related to the mobility and recombination of ions allows the explanation of the Hopf-bifurcation and the calculation of the Hopf frequency f_H of the traveling. In particular, WEM predicts an increasing f_H with the increase of the driving frequency f for $\epsilon_a<0$ while as one approaches $\epsilon_a\approx 0$, f_H practically becomes independent of f. Moreover, f_H depends on the conductivity $\sigma_\perp$, and even more pronouncedly on the sample thickness d since $f_H\propto\sigma_\perp^{-1/2}d^{-3}$. These predictions of the WEM have been checked experimentally in the nematic LCs I52 [13] and Phase 5 [14], and a good quantitative agreement has been found. It has also been shown that the $U_c(f)$ and

*On leave from GDPC Laboratory, Languedoc University of Sciences and Technics, Montpellier, France.

$\mathbf{q_c}(f)$ calculated from the WEM practically coincide with those provided by the SM.

An inspection of the SM shows that the sign (and magnitude) of the two anisotropies, ϵ_a and σ_a, and the initial director alignment are the key parameters when deciding if or what kind of an EC pattern can exist. Consequently it is convenient to categorize the materials as $(-,+)$, $(-,-)$, $(+,+)$ or $(+,-)$ compounds where the first sign corresponds to that of ϵ_a and the second to that of σ_a. Planar $(-,+)$ nematic LCs (i.e., those with $\epsilon_a<0$ and $\sigma_a>0$) are not exclusive targets to investigate electroconvection. There are other combinations of the key parameters where EC can occur either as a direct transition (e.g., homeotropic $(+,-)$ [15]) or as a secondary instability [e.g., homeotropic $(-,+)$ [16,17]], and the SM still can provide a quantitative description of the patterns. These patterns further on will be referred to as standard-EC (s-EC) patterns. The relation between the relevant parameters and the existence of s-EC patterns and their onset behavior has recently been systematically reviewed revealing various s-EC modes in a wide **q** range [18]. It must be noted, however, that according to the rigorous analysis by SM, the boundaries of existence of s-EC modes do not coincide exactly with the sign inversion of the anisotropies [18]. For example, s-EC modes typical in $(-,+)$ compounds cease at reducing σ_a before it reaches zero or, the same mode can survive at increasing ϵ_a up to $(+,+)$ with a small positive ϵ_a.

Contrary to the cases mentioned so far, the existence of s-EC patterns is excluded for substances with $\epsilon_a<0$ and $\sigma_a<0$ [1,18]. This $(-,-)$ combination of the material parameters usually occurs in nematic compounds where at lowering the temperature the sign of σ_a becomes inverted due to an underlying smectic phase. In the higher temperature part of the nematic range these LCs are still $(-,+)$ type, and so s-EC can exist. They become $(-,-)$ only at lower temperatures. There, however, convection in ac electric field associated with roll formation has long ago been observed, e.g., in homologous series of *N*-(*p*-*n*-alkoxybenzylidene)-*n*-alkylanilines, or in di-*n*-4-4′-alkyloxyazoxybenzenes [19,20], and recently in 4-*n*-alkyloxy-phenyl-4-*n*′-alkyloxy-benzoates [21]. The characteristics of these patterns, like orientation of the rolls, contrast, frequency dependence of q_c and U_c, and the director distribution in space and time, are different from those of the s-EC. Since this roll formation process falls outside of the frame of the SM it has been called nonstandard electroconvection (ns-EC) [21]. Though several ideas have been proposed as possible explanations, like a hand-waving argument based on "destabilization of twist fluctuations" [19], a possibility of an isotropic mechanism based on the nonuniform space charge distribution along the field [20,22], and the flexoelectric effect [23], no coherent description has been developed yet.

In this work, we consider a nematic material which is of $(-,-)$ type and exhibits ns-EC patterns in a relatively wide temperature range, though it also becomes $(-,+)$ type showing standard EC close to the clearing point. In Sec. II we introduce the experimental setup and the substance chosen for the investigations. In Sec. III the characterization of the ns-EC patterns is given including the frequency, thickness and temperature dependence of the threshold voltage, wavenumber, and roll orientation, compared to those of s-EC patterns. Section IV presents the results for temperature and/or frequency induced transitions between ns-EC and s-EC. In Sec. V the nonlinear regime above onset is shortly addressed. Section VI is dedicated to the Hopf bifurcation to traveling waves. Finally, in Sec. VII we close the paper with a discussion of the obtained results.

II. SUBSTANCE AND EXPERIMENTAL SETUP

The homologous series of 4-*n*-alkyloxy-phenyl-4-*n*′-alkyloxy-benzoates (labeled as **k/m**, where **k** and **m** are the number of carbon atoms in the alkyloxy chains) offers a large number of liquid crystalline materials which possess nematic as well as smectic phases. We have reported recently [21] that, while their dielectric anisotropy is always negative, carefully selected members of the series exhibit different temperature dependence of the conductivity anisotropy, namely there are compounds which are of $(-,+)$ or $(-,-)$ type in the whole nematic temperature range, as well as those with a sign inversion of σ_a at some temperature in the nematic phase. It has also been shown that in these materials one can conveniently study the temperature induced transition between standard and nonstandard electroconvection. The compound investigated systematically in a previous work (**10/6**) [21] had, however, the disadvantage of a not too wide nematic phase with an even shorter temperature range with $(-,-)$ parameter combination.

The substance used in the present work, 4-*n*-octyloxy-phenyl-4-*n*′-heptyloxy-benzoate (**8/7**), is another member of the same homologous series [24] and has been studied without additional purification or doping. It has a wide nematic range with the phase sequence: isotropic 92 °C nematic 72.5 °C smectic C 62 °C crystalline.

All experiments have been carried out in the nematic phase. In order to ease the comparison with other measurements it is convenient to introduce a reduced temperature as $T^*=(T-T_{NS})/(T_{NI}-T_{NS})$, with T_{NI} and T_{NS} denoting the nematic-isotropic and the nematic-smectic C phase transition temperatures, respectively. This reduced temperature will be used throughout the paper.

The liquid crystal compound has been enclosed between two parallel glass plates coated with etched transparent SnO_2 electrode and rubbed polyimide. Ready-made (EHC Co. Ltd.) planarly aligned cells of different thickness in the range of $3\ \mu m \leq d \leq 50\ \mu m$ have been used. The direction of the director at the surfaces is chosen as the x axis. A sinusoidal ac electric field of frequency f and amplitude $\sqrt{2}U$ has been applied across the sample (along the z axis). Some measurements have also been carried out on a homeotropic (**n** parallel to the z axis) cell of $d=20\ \mu m$.

For electroconvection measurements the cells have been placed into an oven (an Instec hot-stage) thermostatted within ±0.05 °C. EC patterns have been studied with two different setups: polarizing microscopy and laser diffraction. For microscopic observations the patterns have been monitored using either the shadowgraph (single polarizer) tech-

nique or two crossed (or nearly crossed) polarizers. Images have been recorded with a CCD camera, digitized by a frame grabber with a resolution of at least 768×576 pixels and 24 bit color depth, and saved for further processing or analysis. In the diffraction setup a central area of about 1 mm $\times$ 2 mm of the cell has been illuminated with a beam of a laser diode of wavelength $\lambda = 650$ nm. Due to the periodicity of the EC patterns a sequence of diffraction fringes (far field image) appears on a screen placed normal to the initial beam at a distance of $L = 660$ mm from the sample. An optical fiber (with a diameter of 1 mm) has been positioned onto the center of a selected (typically a first order) spot which transmitted the diffracted light into a photomultiplier working in its linear regime. The output of the photomultiplier has been fed through a current-to-voltage converter into a digital oscilloscope. That has allowed computer recording of the fringe intensity with adjustable sampling rate at 8 bit resolution.

Preliminary investigations [21] showed that **8/7** has a long temperature range above T_{NS} where $\sigma_a < 0$, which strongly motivated its use for the present studies. Our recent, aimed measurements in a thick ($d = 50$ μm) sample of **8/7** have revealed that besides $\epsilon_a < 0$ in the whole nematic range, σ_a changes sign at $T^* \approx 0.6$ gaining positive, though small, values for the higher temperature end of the nematic phase. However, we cannot exclude that the sign inversion temperature can be sensitive to the type and amount of uncontrollable ionic impurities, and therefore may somewhat vary for different samples.

III. NONSTANDARD ELECTROCONVECTION—LONGITUDINAL ROLLS

In this section results obtained in the low temperature range of the nematic phase are presented with the aim to characterize the ns-EC patterns appearing at the onset of electroconvection.

A. Contrast and threshold

Upon increasing the applied voltage the nonconventional, ns-EC structure appears in a polarizing microscope in the form of colored stripes (alternating dark and bright stripes at monochromatic illumination) when viewed between crossed (or nearly crossed) polarizers. Though these stripes bear some morphological similarity to the rolls in standard EC, there are two salient differences which are related to the contrast and to the orientation of the pattern. First, using two polarizers is a prerequisite for the detection of the ns-EC pattern. It becomes invisible if one polarizer is removed; i.e., in contrast to s-EC, ns-EC pattern does not produce a shadowgraph image near the onset. Second, the ns-EC stripes run parallel (or nearly parallel) with the initial director **n**, as opposed to the normal or slightly oblique rolls of s-EC. Due to this orientation of the ns-EC stripes we call them longitudinal rolls (LR). We keep the notation parallel rolls (PR) for the case when the stripes are exactly parallel with **n**. A typical snapshot of the LR pattern is shown in Fig. 1.

In addition to its unusual orientation, the pattern is quite weak; the overall contrast is low compared to that of the

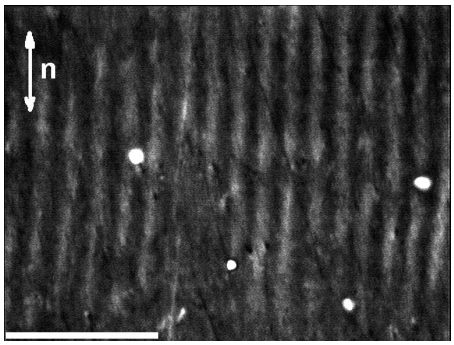

FIG. 1. Snapshot of longitudinal rolls at $T^* = 0.18$, $f = 120$ Hz, and $U = 30.5$ V in a planar cell with $d = 13.2$ μm. A digital contrast enhancement has been applied to the image for better visibility. The scale bar in the lower left-hand corner corresponds to 100 μm, and the double arrow denotes the initial director.

s-EC structure detected in the same cell (see also Fig. 18 in Sec. VII). Figure 2 shows the voltage dependence of the contrast evaluated from a sequence of snapshots taken at increasing and decreasing voltages around the threshold of ns-EC at $T^* = 0.38$ and $f = 60$ Hz using a $d = 12$ μm thick sample. For contrast measurements the recorded images have been converted to gray scale. Taking into account that ns-EC patterns are detected via modulations in the birefringence and that the electric field may induce a change in the birefringence even in the absence of the pattern, the contrast c is defined as the standard deviation of the intensity normalized by the average intensity $\langle I \rangle$, i.e., $c = \sqrt{(I - \langle I \rangle)^2}/\langle I \rangle$. The $c(U)$ curve is continuous; there is no jump or hysteresis at the onset of ns-EC which indicates a forward bifurcation. U_c has been obtained by the common evaluation method, i.e., extrapolating from the linear part of the $c(U)$ curve back to the background contrast level as shown in Fig. 2. The relatively high background contrast level is due to the imperfections in the nematic alignment resulting in birefringence variations. The U_c determined from $c(U)$ actually corresponds to the voltage where the periodic ns-EC pattern becomes visually

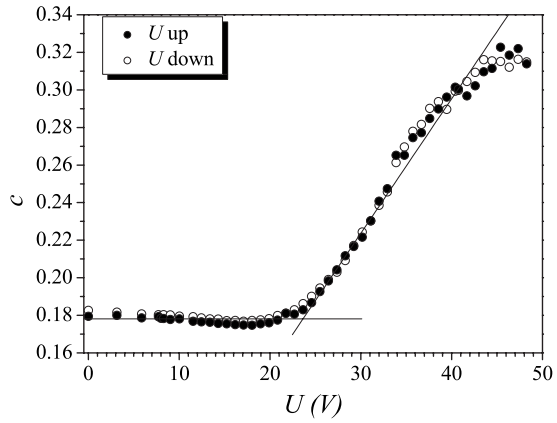

FIG. 2. Contrast as a function of the applied voltage around the onset of the ns-EC instability, measured with increasing (solid circles) and decreasing (open circles) voltages, respectively. $T^* = 0.38$, $f = 60$ Hz, $d = 12$ μm. From the intersection of linear fits, $U_c = 23.6$ V.

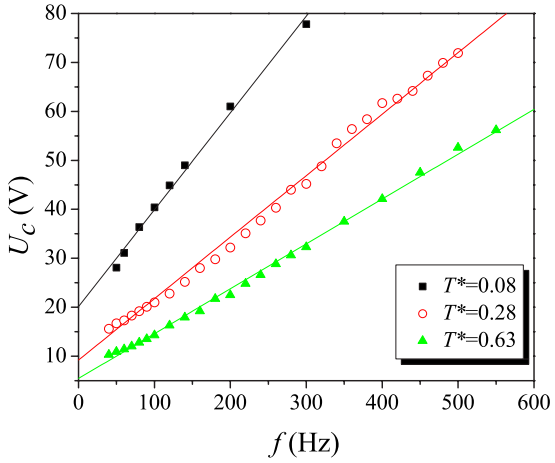

FIG. 3. (Color online) Threshold voltage U_c as a function of frequency f at $T^*=0.08$ (solid squares), $T^*=0.28$ (open circles), and $T^*=0.63$ (solid triangles) in a sample of $d=13.2$ μm. Solid lines represent linear fits to data.

detectable. It is remarkable that the voltage range, where a monotonic (nearly linear) growth of the contrast could be detected, was extremely wide extending to about 20 V above threshold. In terms of the dimensionless control parameter $\varepsilon=(U/U_c)^2-1$ it means that the developing ns-EC pattern remains stable up to $\varepsilon\approx 2$. In contrast to that, in s-EC at much lower ε (≈ 0.1) secondary instabilities and even turbulence can develop.

It must be mentioned that the ns-EC patterns observed in **8/7** are usually not stationary. The stripes are continuously displaced in time; i.e., one has a traveling ns-EC pattern at threshold. To our knowledge this is the first reporting of a Hopf bifurcation in nonstandard electroconvection of $(-,-)$ compounds. Whether the stripes travel or not, it does not affect the method of the threshold characterization of the pattern which is based on the analysis of snapshots. Peculiarities related to the Hopf bifurcation will be discussed separately in Sec. VI.

In the lower temperature region of the nematic phase LR appears at the onset of ns-EC in the whole studied frequency range. Figure 3 exhibits the frequency dependence of U_c of ns-EC patterns at three different temperatures ($T^*=0.08$, $T^*=0.28$, and $T^*=0.63$) for a $d=13.2$ μm thick sample. It is obviously seen that U_c increases linearly with the frequency as demonstrated by the fits in Fig. 3. This again is in contrast to the situation in s-EC where the $U_c(f)$ curve either grows rapidly approaching the cutoff frequency f_c (for the conductive regime), or follows a $U_c\propto\sqrt{f}$ behavior (in the dielectric regime) [2]. It is also seen that both the absolute value of U_c and the steepness of the $U_c(f)$ curves decrease with increasing temperature.

In Fig. 4 the thickness dependence of U_c is plotted at a fixed reduced temperature $T^*=0.38$. It is seen that the threshold voltage scales with d as indicated by the one-parameter linear fit; i.e., the ns-EC patterns have a threshold electric field instead of a threshold voltage. This holds for other frequencies and temperatures too, and agrees with previous results on ns-EC patterns observed in other $(-,-)$ substances [19,20,23,25]. This behavior is in contrast to that of the conductive regime of s-EC where U_c is independent of d, and it resembles the dielectric regime of s-EC which, according to the rigorous theoretical analysis, also has $U_c\propto d$ in certain approximations, namely for not too low and not too high f and d [2].

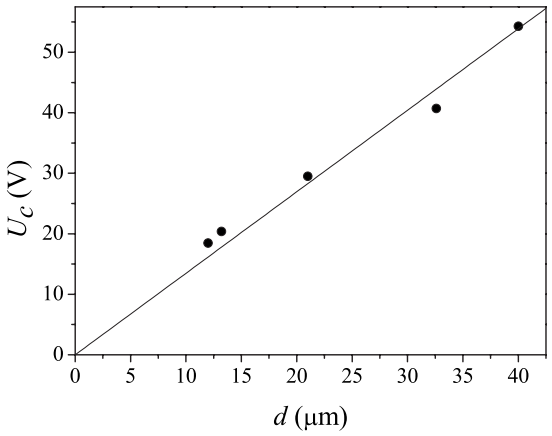

FIG. 4. Threshold voltage U_c versus sample thickness d at $f=30$ Hz for reduced temperature $T^*=0.38$. Solid line represents a one-parameter linear fit.

B. Wavelength and orientation

Besides the threshold voltage, the critical wave vector of the LR pattern has also been determined by measuring the wavelength λ as well as the orientation of the stripes. In order to help comparison of cells of different thicknesses, a dimensionless wave number $q_c=2d/\lambda$ has been introduced. The frequency dependence of q_c is plotted in Fig. 5 for ns-EC in a $d=13.2$ μm thick sample at a relatively low temperature ($T^*=0.28$). At this particular thickness the wavelength is comparable to d. At low frequencies (up to $f\approx 150$ Hz in Fig. 5) q_c seems to be frequency independent, then it grows linearly with f just as $U_c(f)$ does. This feature is different from that of the conductive s-EC where q_c and U_c are characterized by similar nonlinear frequency dependencies.

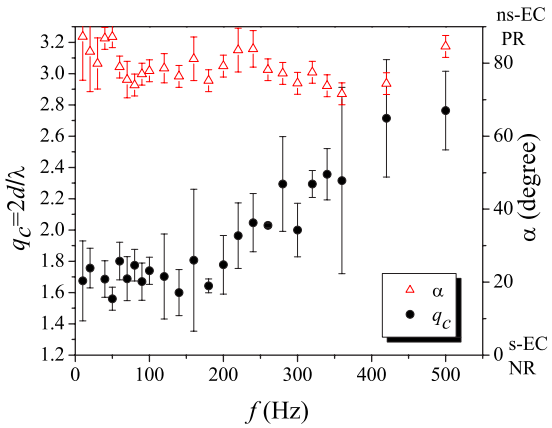

FIG. 5. (Color online) Frequency dependence of the dimensionless wave number q_c (solid circles) and that of the angle α between $\mathbf{q_c}$ and $\mathbf{n}$ (open triangles) at $T^*=0.28$ in a $d=13.2$ μm thick sample.

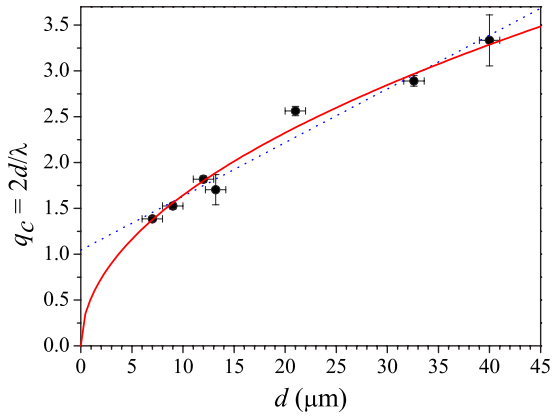

FIG. 6. (Color online) Dimensionless wave number q_c as a function of the sample thickness d at $T^*=0.23$ and $f=30$ Hz. The solid line is single-parameter square-root fit, while the dotted line is a linear fit.

The orientation of the ns-EC pattern is best represented by the angle α between the wave vector $\mathbf{q_c}$ and $\mathbf{n}$. According to this definition $\alpha=0$ characterizes the s-EC normal rolls, while $\alpha=90°$ corresponds to exactly parallel rolls (ns-EC PR). The frequency dependence of α is also plotted in Fig. 5. One can see that at the selected temperature (and at low temperatures in general) α shows only a slight dependence on f: $\mathbf{q_c}$ is practically perpendicular to $\mathbf{n}$ (PR) at low frequencies, then α fluctuates around 80°; i.e., in the whole frequency range one has ns-EC LR pattern at the onset. Despite of the kink in $q_c(f)$, the nearly constant $\alpha(f)$ excludes the existence of a Lifshitz point.

The large error bars in Fig. 5 indicate a bigger scatter of the measured q_c and α than found usually in s-EC. This insinuates that besides the lower contrast, the ns-EC patterns are less regular at onset than the typical s-EC ones which is manifested in the spatial variation of the wavelength λ as well as of the orientation of the stripes [cf. Figs. 7(a) and 7(c) in Sec. IV below]. This is an inherent property of the structure and presumably results from a shallower wave-number band of the neutral surface [2] compared to s-EC. A coarsening process leading to more regular patterns required hours.

In Fig. 6 q_c of the ns-EC stripes is plotted as a function of the sample thickness at the reduced temperature $T^*=0.23$ and $f=30$ Hz. Note that q_c increases with the increase of d. The depicted behavior is different from that of the s-EC state, where on the one hand, in the conductive regime the wavelength is proportional to the thickness hence q_c is a constant [4]. On the other hand, in the dielectric s-EC regime λ is independent of d, thus the dimensionless q_c is proportional to the cell thickness. We note that this holds theoretically for specific approximations and experimentally fulfills for a rather broad range of thicknesses (except for extremely small and large d). The thickness dependence of q_c for the ns-EC of **8/7** does not match any of the behavior mentioned above. Experimental data can be reasonably well fitted either with a linear (however, not proportional relation—the dotted line in Fig. 6 extrapolates to an offset $q_c \approx 1$ at $d=0$) or with a single-parameter square-root dependence (solid line), i.e., the curves corresponding to the two fit types do not differ significantly in the experimentally available thickness range. For the motive of considering a square-root dependence of q_c on d see discussion later in Sec. VII.

In an attempt to broaden the thickness range for the investigation thicker ($d=50$ μm) and thinner ($d=3.4$ μm) samples have also been prepared. In the thicker cell, however, not only the thresholds have become higher but the contrast of the pattern has been found too low for measuring q_c with sufficient precision. On the other hand, in the thinner sample no pattern has been observed in the frequency range of our interest, i.e., below approximately 100 Hz [26]. This may be related to the short director relaxation time which in thin samples becomes comparable with the charge relaxation time and thus prevents the formation of space charges necessary for EC [27].

C. Flow

The LRs of ns-EC are unequivocally associated with flow vortices. This can be seen when observing the motion of dust particles (or of polystyrene spheres embedded into the nematic intentionally). A circular particle motion typically occurs in the plane normal to the stripes; the particles go out from, and come back into focus within the length scale of the wavelength.

One must mention, however, that some irregular motion of particles, involving both rotation and large-scale (compared to λ) translation, becomes detectable already at U_{pm}, far (typically by a few volts, depending on T^* and f) below the ns-EC threshold voltage U_c. This holds for the whole temperature range of ns-EC. The particle motion looks similar to that found below the threshold of the so-called prewavy pattern in traditional $(-,+)$ nematics [28]. The particle motion can be traced at increasing temperatures up to and even through the nematic-isotropic transition. U_{pm} is a monotonically decreasing function of T^* without any discontinuity at T_{NI} similarly to some observations in other $(-,+)$ nematics [29]. Irregular particle motion has also been observed below U_c of s-EC in **8/7** (at high temperatures—see next section), however, in this case U_{pm} has been found very close to the s-EC threshold (less than 1 V below U_c).

IV. TEMPERATURE AND FREQUENCY INDUCED TRANSITION BETWEEN s-EC AND ns-EC

Temperature has a significant effect on the morphology of the EC patterns. The nematic range of **8/7** can be subdivided into three regions: the low and the high temperature ends, and the intermediate range. Figure 7 shows snapshots of the typical patterns (taken above threshold at $\varepsilon \approx 0.2$ for a better contrast) while Fig. 8 exhibits characteristic $U_c(f)$ curves from each region.

The results presented in the preceding section have been obtained in the lower half of the nematic temperature range ($T^* \lesssim 0.5$) where ns-EC patterns (PR or LR) have been observed at all studied frequencies [Fig. 7(a)]. At those temperatures the substance belongs to the $(-,-)$ class of materials.

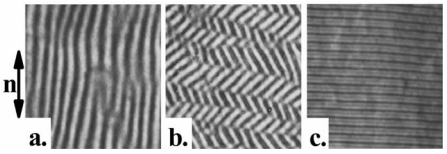

FIG. 7. Snapshots of EC patterns taken with nearly crossed polarizers above the threshold ($\varepsilon \simeq 0.2$) in a cell of $d=12$ μm. (a) Longitudinal rolls at $T^*=0.38$, $f=50$ Hz; (b) zig-zag domains of oblique rolls at $T^*=0.54$, $f=30$ Hz; (c) normal rolls at $T^*=0.95$, $f=90$ Hz. The pictures depict a cell area of 225 μm$\times$225 μm; the initial director is vertical.

At high temperatures ($T^* \gtrsim 0.85$) however, the sign of σ_a is positive, and the material becomes $(-,+)$ type. Thus, it is not surprising that in this temperature range s-EC rolls have been observed [Fig. 7(c)]. At $T^*=0.9$ conductive oblique, then normal rolls appear with increasing frequency at the onset, while above $f_c \approx 550$ Hz dielectric rolls set in. The crossover from conductive (solid triangles) to dielectric (open triangles) s-EC patterns is clearly seen in the $U_c(f)$ curve presented in Fig. 8. Characteristics of these patterns match perfectly with those of the s-EC patterns seen in standard $(-,+)$ nematics: they are detectable with shadowgraph, have a high contrast, and $U_c(f)$ and $\mathbf{q}_c(f)$ follow the theoretical predictions of the SM.

The middle temperature range ($0.5 \lesssim T^* \lesssim 0.85$)—which includes the sign inversion point of σ_a—offers a greater variety of pattern morphologies. In a large part of this intermediate temperature range a crossover from s-EC to ns-EC occurs with the increase of the frequency. It is demonstrated in Fig. 8 which shows the $U_c(f)$ dependence for s-EC by solid, and for ns-EC by open circles at $T^*=0.84$. We note here that the frequency dependence of the ns-EC threshold at $T^*=0.84$ fits into the trend obtained for ns-EC at lower temperatures (Fig. 3 of Sec. III A): $U_c(f)$ is linear, and both the

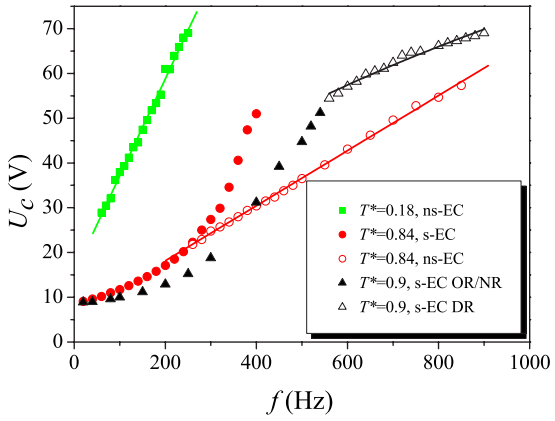

FIG. 8. (Color online) Frequency dependence of the threshold voltage U_c of ns-EC longitudinal rolls at $T^*=0.18$ (squares), s-EC (solid circles), and ns-EC patterns (open circles) at $T^*=0.84$ and s-EC conductive (solid triangles) and dielectric (open triangles) rolls at $T^*=0.9$ in a sample of $d=13.2$ μm. The solid lines at $T^*=0.18$ and $T^*=0.84$ are linear fits to ns-EC threshold data. The curve on data at $T^*=0.9$ is a square-root fit for the dielectric s-EC threshold.

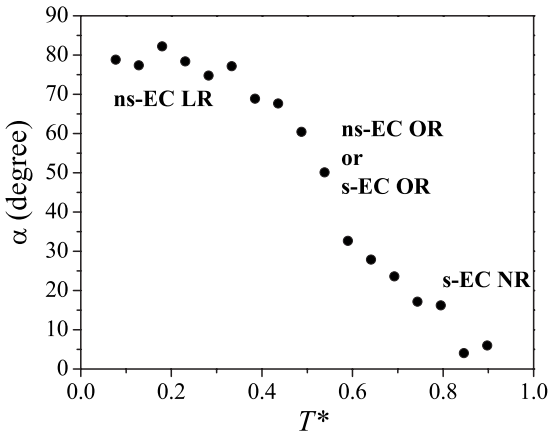

FIG. 9. Temperature dependence of the angle α between the wave vector $\mathbf{q_c}$ and the initial director $\mathbf{n}$ at $f=60$ Hz in a $d=12$ μm thick sample.

absolute value of U_c and the slope of $U_c(f)$ decrease with increasing temperature. It is also seen in Fig. 8 that there is a frequency range where a transition from ns-EC to s-EC could be induced (as a secondary instability) with the increase of the driving voltage U. Further details of that behavior will be discussed later in Sec. V.

The most representative patterns of the intermediate temperature region are oblique rolls [Fig. 7(b)] with temperature and frequency dependent obliqueness. Figure 9 shows the obliqueness angle α as a function of temperature at $f=60$ Hz in a $d=12$ μm thick sample. At low temperatures $\alpha \approx 80°$ is found which is characteristic of the ns-EC: the stripes are almost parallel with the initial director [Fig. 7(a)]. In the intermediate temperature range α decreases from $\approx 70°$ to $\approx 20°$ and zig-zag domains become typical [Fig. 7(b)]. At high temperatures α reaches zero indicating s-EC normal rolls.

It must be noted that oblique rolls (zig-zag domains) can occur both in ns-EC and in s-EC. Though ns-EC patterns typically have bigger α than those of s-EC, the two types of patterns cannot simply be distinguished entirely by the magnitude of α. In addition, at some thickness range ($d \approx 10$ μm), even the wave number q_c of the two kinds of patterns is very similar. Therefore, in those cases in the intermediate temperature range the presence or the absence of the shadowgraph image at onset is the only decisive property between the s-EC and ns-EC, respectively. As the thickness dependence of q_c differs for the two types of patterns (see discussion in Sec. III B), at large enough cell thicknesses (e.g., at $d=40$ μm) the temperature induced morphological changes yield also a jump in q_c as shown in Fig. 10. For this sample thickness the wavelength of ns-EC patterns is considerably smaller than d and interestingly, q_c does not seem to depend on the temperature. This is rather surprising, since in this relatively wide temperature range (≈ 15 °C) the material parameters of **8/7** change considerably [see, e.g., Fig. 1(b) and Fig. 2 in [21]].

Finally, it must be noted that the three temperature ranges discussed above do not have sharp boundaries—the transition from one to the other is practically continuous. More-

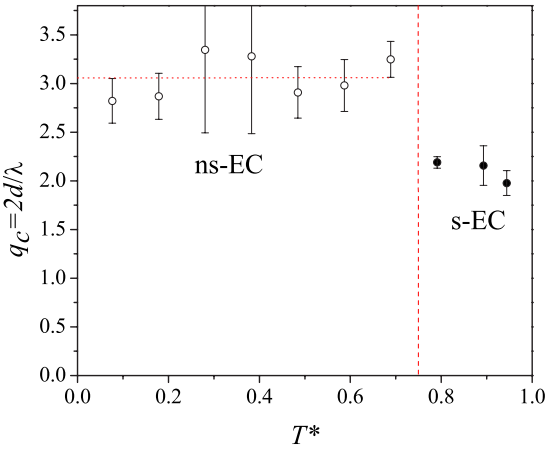

FIG. 10. (Color online) Temperature dependence of the dimensionless wave number q_c at $f=40$ Hz in a $d=40$ μm thick sample. The dotted line is the mean value of q_c in the ns-EC temperature region.

over, in different samples these boundary regions have been found to vary slightly, presumably due to minor variations of the material parameters, among cells of different thickness or preparation method.

V. ELECTRIC FIELD AS A SWITCH BETWEEN s-EC AND ns-EC

It has been shown in Sec. III A that the ns-EC PR patterns observed at low temperatures do not suffer morphological changes (apart from a monotonic increase of the contrast) in a wide voltage range above onset. At very high voltages ($\varepsilon \gtrsim 2$), however, a transition to turbulence can be observed which is detectable with shadowgraph.

At high temperatures for s-EC the regular nonlinear behavior is detected—appearance of defects then defect chaos and turbulence, occurring already at voltages not too far above the threshold.

The situation is quite different for the intermediate temperature range ($0.5 \lesssim T^* \lesssim 0.85$) where oblique stripes appear at onset as demonstrated in Figs. 7(b) and 9. These patterns have been identified as ns-EC OR due to the absence of shadowgraph images. Increasing the voltage, however, a transition from ns-EC to s-EC could be induced. The transition involves a gradual change of both the angle α and the dimensionless wave number q, from ns-EC OR (large obliqueness) via s-EC OR (smaller α) to s-EC NR ($\alpha=0$). The rotation of the roll direction is clearly demonstrated in Fig. 11 by the photographs of the diffraction fringes taken at increasing voltages.

Figure 12 exhibits data extracted from the diffraction measurements showing that both q and α vary continuously with the applied voltage. At even higher voltages the usual defect chaos is observed.

Figure 13 shows snapshots of the patterns in the same sample, taken at the same T^* and f as the diffraction fringes in Fig. 11. The main features of the dependence of α and q on the voltage are again demonstrated: α decreases and q slightly increases with the increase of ε.

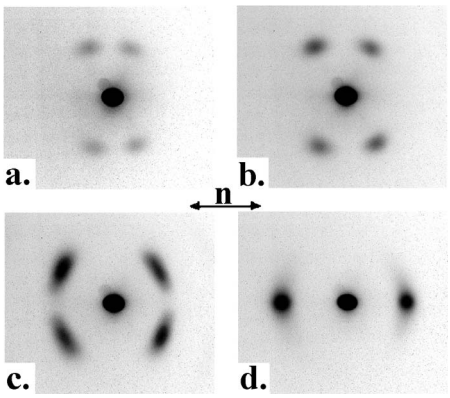

FIG. 11. Diffraction fringes in a $d=12$ μm thick sample at $T^*=0.64$, $f=30$ Hz and (a) $U=11.13$ V ($\varepsilon=0$), ns-EC OR; (b) $U=12.16$ V ($\varepsilon=0.19$), ns-EC OR; (c) $U=14.6$ V ($\varepsilon=0.72$), s-EC OR; (d) $U=17.7$ V ($\varepsilon=1.53$), s-EC NR. A digital contrast enhancement of the images has been performed for better visibility.

VI. TRAVELING WAVES IN ns-EC

It was mentioned in Sec. III A that the ns-EC patterns appearing at onset are not stationary. Instead, the rolls travel; i.e., a Hopf bifurcation occurs. That holds for almost the whole (f, T^*, d) parameter-space covered by our measurements, except a few narrow parameter ranges which will also be discussed later in this section.

The temporal evolution of the patterns (i.e., the displacement of rolls) are best demonstrated in space-time images where the tilt angle is related to the velocity of traveling. In Fig. 14 we give a few examples of space-time images for patterns of different kind recorded in a $d=13.2$ μm thick sample.

Comparing various pattern types it was found that the ns-EC stripes in the low temperature range of the nematic phase travel the fastest [Fig. 14(a)]. In the high temperature range (very close to $T^*=1$) at low frequency the s-EC oblique rolls do not travel [Fig. 14(b)]. The s-EC normal rolls at frequencies above the Lifshitz point f_L (≈ 170 Hz at $T^*=0.99$ in the $d=13.2$ μm sample), however, travel too [Fig. 14(c)], but their traveling speed is much smaller than that of the ns-EC stripes [note the different time scales in Figs. 14(a) and 14(c)].

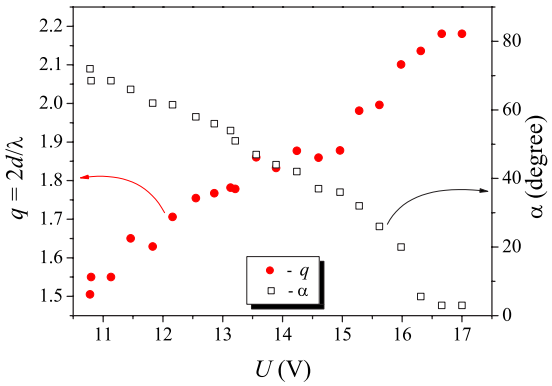

FIG. 12. (Color online) Obliqueness angle α and the dimensionless wave number q as a function of the applied voltage U at $T^*=0.64$, $f=30$ Hz, and $d=12$ μm.

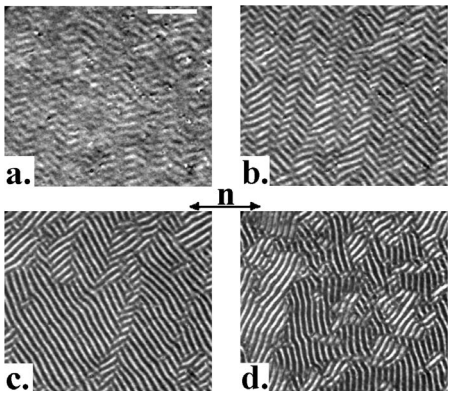

FIG. 13. Snapshots of patterns taken through a polarizing microscope, demonstrating the voltage dependence of the obliqueness of the rolls in a $d=12$ μm thick sample at $T^*=0.64$, $f=30$ Hz and (a) $\varepsilon=0$, ns-EC OR; (b) $\varepsilon=0.39$, ns-EC OR; (c) $\varepsilon=0.75$, s-EC OR; (d) $\varepsilon=1.27$, s-EC OR. A digital contrast enhancement of the snapshots has been performed for better visibility. The scale bar in (a) denotes 100 μm.

In Fig. 15 the dependence of the Hopf frequency $f_H=v_n/\lambda$ on the driving frequency f has been plotted both for the low [Fig. 15(a)] and for the high [Fig. 15(b)] temperature range measured in a $d=40$ μm thick sample. Here v_n denotes the traveling velocity of the stripes perpendicular to their orientation. In the low temperature range, where only ns-EC has been detected, f_H increases monotonically with the increase of f [Fig. 15(a)].

At higher temperatures, where the s-EC to ns-EC transition takes place at increasing f [indicated by arrows in Fig. 15(b)], however, another behavior was found. At low f, where s-EC is observed, the $f_H(f)$ dependence is *not* a monotonic function. Increasing the frequency f_H reaches a small maximum and then decreases as we approach the frequency at which the s-EC to ns-EC transition occurs. In the close neighborhood of the transition frequency $f_H=0$ both for s-EC and ns-EC. With further increase of f, where ns-EC takes over, $f_H(f)$ becomes linear within the experimental error—as

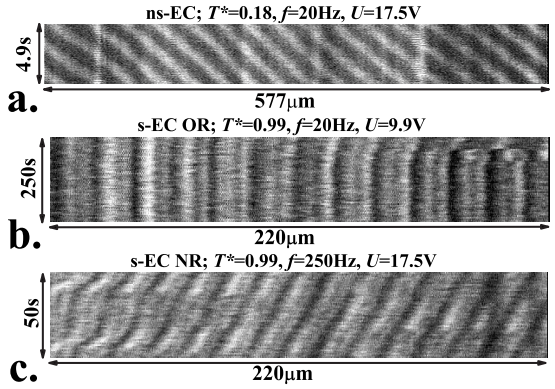

FIG. 14. Space-time images at onset of EC in a $d=13.2$ μm thick sample. Spatial and temporal scales as well as T^*, f, and U are indicated for each image which represent examples of (a) ns-EC PR; (b) s-EC OR; (c) s-EC NR patterns, respectively. A digital contrast enhancement of the snapshots has been performed for better visibility.

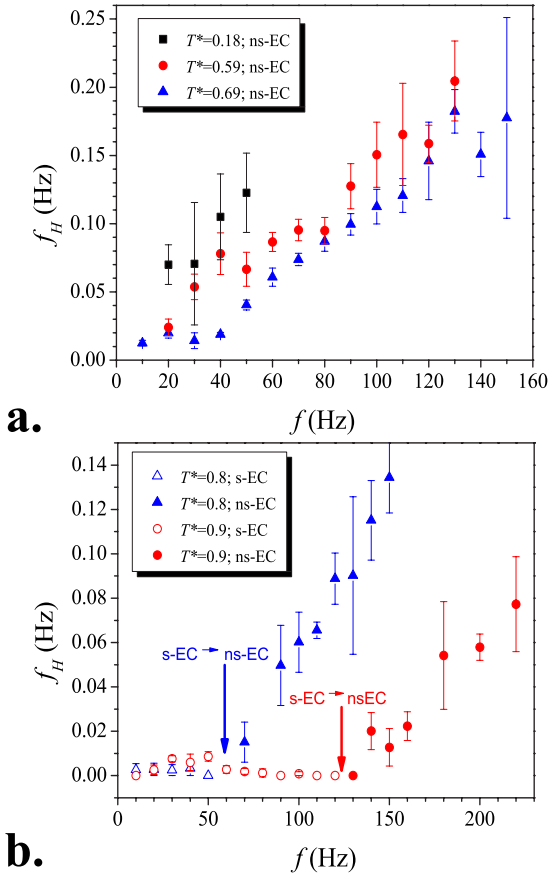

FIG. 15. (Color online) Hopf frequency f_H, measured in a $d=40$ μm thick sample, as a function of the driving frequency f (a) in the low temperature range (at $T^*=0.18$, 0.59, and 0.69) where only ns-EC is observed; (b) in the upper end of the intermediate temperature range (at $T^*=0.8$ and 0.9) where both s-EC and ns-EC are observed (arrows indicate the frequencies where the s-EC to ns-EC transition is detected).

was found at low temperatures—with a slope decreasing with temperature. Note that in general (similarly to the 13.2 μm thick sample) f_H is much larger in ns-EC than in s-EC.

The temperature dependence of f_H, measured at $f=50$ Hz is shown in Fig. 16. It is seen that f_H has a maximum near the middle of the nematic temperature range. For higher T^*, however, approaching the ns-EC to s-EC transition f_H decreases to zero. Above the ns-EC to s-EC transition temperature s-EC rolls start to travel again, with considerably smaller f_H than that measured for ns-EC. Close to the nematic to isotropic phase transition temperature (at $T^*>0.94$ in the $d=40$ μm sample at $f=50$ Hz), s-EC rolls become stationary ($f_H=0$) again.

The Hopf frequency is very sensitive to the sample thickness. For illustration we present in Fig. 17 the $f_H(f)$ curves for two samples of different thickness ($d=13.2$ μm and 40 μm, respectively) at $T^*=0.18$ (where only ns-EC is present). For both thicknesses f_H increases with the increase of f, though the available frequency range is much smaller in the thicker cell. We want to note here that ns-EC patterns are much easier to observe in thin ≈ 10 μm samples than in

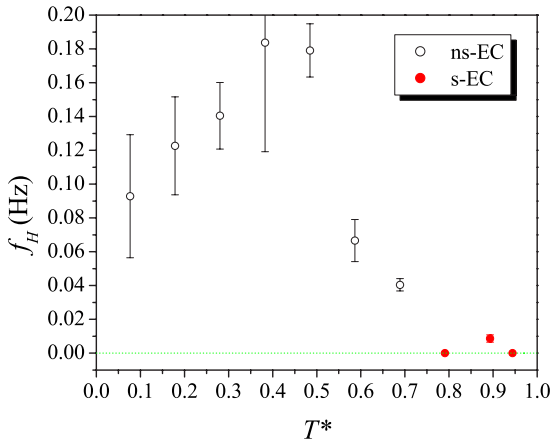

FIG. 16. (Color online) Temperature dependence of the Hopf frequency f_H measured in a $d=40$ μm thick sample at $f=50$ Hz.

thicker (≈ 40 μm) ones because of the higher contrast in thinner cells. On the other hand, in thinner samples f_H is larger and its experimental error is also considerably larger (cf. error bars for data measured in $d=13.2$ μm and in $d=40$ μm samples in Fig. 17) due to the finite sampling rate of our image recording system. Additionally, the already mentioned larger spatial variations of q_c and α in ns-EC compared to those in s-EC also contribute to a much larger experimental error for ns-EC f_H data [see Fig. 15(b)].

At present, the weak electrolyte model (WEM) developed for s-EC is the only theoretical approach which can account for traveling waves in electroconvection of nematics. WEM predictions provide a relation $f_H \propto U_c^2/(d^3\sigma_\perp^{1/2})$ [14]. Since, as we have shown, ns-EC has a field threshold E_c, the WEM relation translates into $f_H \propto E_c^2/(d\sigma_\perp^{1/2})$. For a comparison with the experimental data, we assume that the conductivity is the same in both cells, and insert the measured E_c values into the relation. Then, the calculated ratio of the Hopf frequencies becomes $f_H|_{13.2\ \mu m}/f_H|_{40\ \mu m} \approx 3$. On the other hand, data in Fig. 17 at $f=40$ Hz provide $f_H|_{13.2\ \mu m}/f_H|_{40\ \mu m} = 6.0 \pm 2.4$. One must note that the comparison is limited to a narrow frequency range, 20 Hz $\leq f \leq$ 50 Hz, where data exist

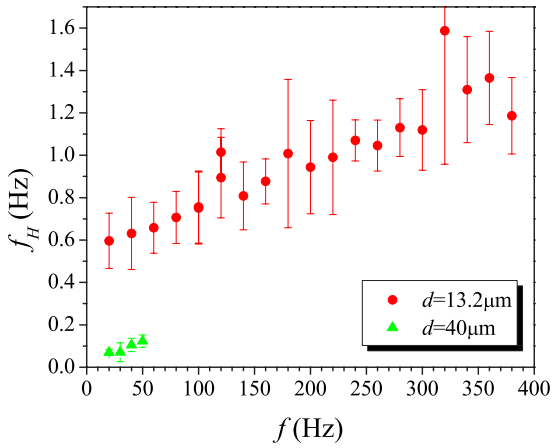

FIG. 17. (Color online) Dependence of the Hopf frequency f_H on the driving frequency f measured at $T^*=0.18$ in two samples of different thickness $d=13.2$ μm and 40 μm.

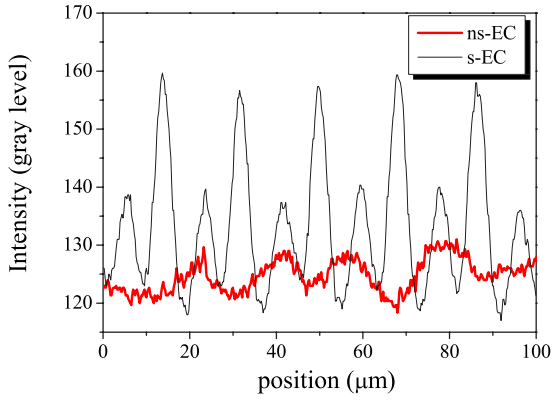

FIG. 18. (Color online) Intensity profiles (on a 256 gray level scale) obtained along a line perpendicular to the rolls for s-EC (at $f=20$ Hz, $U_c=9.8$ V) and for ns-EC (at $f=60$ Hz, $U_c=10.4$ V) patterns. $T^*=0.83$ and $d=13.2$ μm.

for both cell thicknesses. As the experimental and calculated ratios are not far from each other—taking into account that the actual electrical conductivities of the cells have not been measured subsequently—one can anticipate that the WEM may be the appropriate model to explain Hopf bifurcation in ns-EC too. The exploration of the precise scaling of f_H with d would require, however, additional aimed measurements.

VII. DISCUSSION

In the preceding sections we have attempted to give a full experimental characterization of the electroconvection patterns in the nematic **8/7** bringing the properties of ns-EC patterns into prominence. Let us summarize their most important characteristics emphasizing those which differ from the s-EC ones and discuss some of their consequences.

(i) ns-EC patterns have been observed in substances of $(-,-)$ type. The pattern near onset cannot be visualized by shadowgraph imaging; i.e., no focusing or defocusing effects act. Instead, crossed (or nearly crossed) polarizers are needed for the detection of the modulations in birefringence. In addition one observes flow dynamics below the threshold where the genuine ns-EC patterns become detectable. The pattern remains stable above threshold over an unusually broad voltage range up to the appearance of the turbulent state (typically at about $\varepsilon \approx 2$). The pattern is less regular due to spatial variations of $\mathbf{q}$ which indicates a quite broad wavenumber band (i.e., a shallow neutral surface). The overall contrast is low and does not exhibit a sharp increase at onset—see Figs. 18 and 19, and the discussion below for more details.

The low overall contrast of the ns-EC pattern compared to that of the s-EC structure can well be demonstrated in the intermediate nematic temperature range of **8/7**, where both patterns appear and one can switch from one to the other by changing *only* the frequency and tuning the voltage to the threshold value. Figure 18 shows the intensity profiles of the transmitted light along a line perpendicular to the direction of s-EC (at $T^*=0.83$ and $f=20$ Hz) and of ns-EC (at $T^*=0.83$ and $f=60$ Hz) from snapshots taken at the onset with

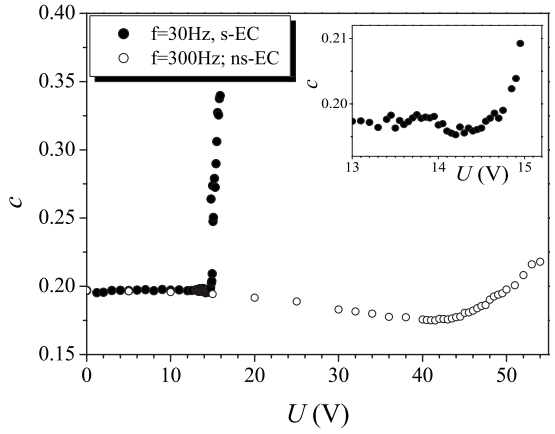

FIG. 19. Contrast as a function of the applied voltage measured in a $d=13.2$ μm sample of **8/7** at $T^*=0.67$ for the s-EC instability ($f=30$ Hz, closed circles) and for the ns-EC instability ($f=300$ Hz, open circles). The inset is a blow-up around the onset of the s-EC instability.

identical (nearly crossed) polarizer settings. The s-EC pattern is sharper; its intensity profile is periodic, and the intensity oscillations are large. On the contrary, the ns-EC pattern is not strictly periodic, and its intensity modulation has a much smaller amplitude which is almost comparable to background intensity variations.

Similarly, in the intermediate temperature range it is possible to compare directly the voltage dependence of the contrast $c(U)$ for s-EC and ns-EC by changing the frequency and holding all other parameters (T^* and d) and conditions (i.e., polarizer positions, illumination, etc.) fixed. Such a comparison has been done in a $d=13.2$ μm thick sample at $T^*=0.67$ and the results are displayed in Fig. 19. As one can see, the increase of c at the onset is much sharper for s-EC compared to that for ns-EC. Above the threshold, there is a linear part of the $c(U)$ curve for both s-EC and ns-EC where the developing pattern remains stable. However, in this linear range c for s-EC increases by $\approx 70\%$ within only $\varepsilon \approx 0.1$ while, c for ns-EC increases only by $\approx 20\%$ within $\varepsilon \approx 0.4$. This again demonstrates that the contrast of the ns-EC pattern is weak (compared to that of the s-EC pattern) and that the ns-EC pattern remains stable over a broad voltage range.

One must note one more characteristics of the $c(U)$ curves displayed both in Fig. 19 and in Fig. 2: just below the onset of ns-EC there is a shallow, however, broad ($\approx 10-15$ V) minimum of $c(U)$ covering the voltage range where motion of (dust) particles has been optically detected. Similarly, in the s-EC regime there is also an indication of an even shallower minimum covering a narrow (≈ 0.5 V) voltage range just below onset—see the inset in Fig. 19. This is again in accordance with our microscopic observations described in Sec. III C and is presumably related to the influence of the electric field on the not perfectly homogeneous basic state ($c \approx 0.2$ without electric field—see Fig. 19). At the voltage U_{pm}, the overall mean value of the transmitted light intensity slightly increases due to nonperiodic (both in space and in time) modulations of the birefringence. On the other hand, the standard deviation of the transmitted light intensity remains constant while passing through U_{pm}, and it starts to increase at a higher voltage close to U_c.

(ii) The threshold voltage is proportional to the cell thickness in the experimentally studied range; thus the instability is characterized by a critical electric field. The threshold voltage is a linear function of the driving ac frequency. The critical wavelength does not scale with the cell thickness. The director oscillates with the applied ac frequency. This latter statement is based on our measurements of the temporal evolution of the diffracted light intensity, and holds for stationary ns-EC patterns only [for **8/7** in a very limited (f, T^*, d) parameter space]. In the majority of the (f, T^*, d) parameter space for **8/7**, and for other nematic liquid crystals, whenever Hopf bifurcation occurs at the onset, traveling waves presumably brake the symmetry of the system and the temporal dependence of the diffracted light intensity becomes more complex representing a subject of an ongoing investigation [34].

This group of properties strongly indicates that ns-EC has characteristics reminiscent of the dielectric regime of electroconvection, though occurring at unusually low frequencies. One can easily perform a test, e.g., for MBBA material parameters with very low conductivity, in order to push the dielectric regime toward low frequencies. The linear stability analysis obviously delivers the standard dielectric mode with normal rolls (U_c and q_c are square-root functions of f, and $\alpha=0$). However, changing the sign of σ_a, i.e., imitating the property of **8/7**, the same linear stability test does not allow for any pattern (there is no finite threshold) in the whole frequency range.

(iii) The stripes of the pattern align parallel or at a small angle to the basic director alignment (longitudinal rolls).

Longitudinal domains (similar in appearance to the ns-EC discussed here) have been reported earlier in a few nematics under other conditions, namely at dc or very low frequency (up to few) Hz: ac driving [30–32]]. This pattern formation has been explained as a static director deformation of flexoelectric origin which does not involve flow and whose threshold field strongly depends on f [32]. We should emphasize, however, that such patterns at dc voltages have not been observed in **8/7**, and in addition, flow always formed an integral part of the ns-EC patterns. Nevertheless, the direction of the rolls suggests that flexoelectricity may play a role in the ns-EC mechanism.

Going on with the above linear stability analysis and adding a flexoelectric term with literature coefficients for MBBA to the free energy density and performing the test for $\sigma_a<0$ one obtains a high, but finite EC threshold with a high roll obliqueness. It shows that the extension of the SM of EC by incorporating flexoelectricity is sufficient to provide a finite threshold for a pattern of dielectric time symmetry in $(-,-)$ substances [33]. Further theoretical studies show that flexoelectricity does not allow the usual decoupling of spatial modes and temporal symmetries separating the scenarios into conductive and dielectric modes [35]. Flexoelectricity leads to coupled modes in the whole frequency range. These preliminary calculations suggest that extending the SM by flexoelectricity is a very good candidate to account for the observed pattern formation. We hope that a fine-tuning of the model with measured material parameters will yield a full quantitative agreement with the experiments. Some related calculations [33] also proposed that in such a flexo-dielectric

pattern one might have a $q_c \propto \sqrt{d}$ dependence, which justifies our test for a square root fit in Fig. 6.

We have shown that the longitudinal domains can be traveling; i.e., the ns-EC stripes may arise in a Hopf bifurcation. Actually in **8/7** traveling waves have been observed instead of stationary patterns in almost the whole (f, T^*, d) parameter space. The Hopf frequencies measured for the ns-EC pattern were considerably higher than f_H for the s-EC rolls of **8/7**, but were of the same order of magnitude that had been found in the conventional $(-,+)$ nematic I52 [13]. There were no indications that the main characteristics $(U_c, \mathbf{q_c})$ of the traveling ns-EC pattern differ significantly from those of stationary ns-EC [measured in **8/7** under specific conditions in the (f, T^*, d) space or in **10/6** [21]]. Therefore we anticipate that, once the instability mechanism of the stationary ns-EC pattern will be completely understood, the traveling will be possible to be explained by adding WEM effects.

Besides the nonzero f_H a significant difference between traveling and stationary patterns could only be detected in the temporal evolution of the diffracted fringe intensities. For conductive s-EC traveling leads to the considerable increase of the $2f$ intensity modulation, while for ns-EC it seemingly yields a reduction of the modulation amplitude [34]. Clarification of this problem would need further experimental investigations on various pattern types, as well as theoretical studies of the temporal evolution of the director profiles and the diffraction optics.

Though all measurements presented in this paper have been carried out using planar **8/7** cells, homeotropic samples have also been tested. No direct transition from the spatially homogeneous homeotropic to a patterned EC state could be observed. Upon increasing voltages a bend Freedericksz transition was first detected as the primary instability at $U_F \approx 5$ V. At voltages above U_F, however, all ns-EC and s-EC scenarios discussed above could be identified. Main characteristics of the patterns in the homeotropic cells were similar to those of the planar ones, except that the patterns were disordered and even less sharp. It indicates that the homeotropic ns-EC in $(-,-)$ is practically driven by the planar instability mechanism (via the Freedericksz distorted quasiplanar layer in the middle of the homeotropic cell), just as it is the case in the homeotropic s-EC of regular $(-,+)$ compounds.

ACKNOWLEDGMENTS

The authors thank W. Pesch and A.P. Krekhov for fruitful discussions. The authors are grateful to G. Pelzl for providing the substance. Financial support by Hungarian Research Contracts Nos. OTKA-K61075, OTKA T-037336, NKFP-128/6 and the EU network PHYNECS is gratefully acknowledged.

[1] P. G. de Gennes and J. Prost, *The Physics of Liquid Crystals* (Claredon, Oxford, 1993).
[2] L. Kramer and W. Pesch, in *Pattern Formation in Liquid Crystals*, edited by Á. Buka and L. Kramer (Springer-Verlag, New York, 1996), p. 221.
[3] L. Kramer and W. Pesch, in *Physical Properties of Nematic Liquid Crystals*, edited by D. A. Dummur, A. Fukuda, and G. R. Luckhurts (Inspec, London, 2001), p. 441.
[4] E. Bodenschatz, W. Zimmermann, and L. Kramer, J. Phys. (France) **49**, 1875 (1988).
[5] S. Rasenat, G. Hartung, B. L. Winkler, and I. Rehberg, Exp. Fluids **7**, 412 (1989).
[6] S. Rasenat, V. Steinberg, and I. Rehberg, Phys. Rev. A **42**, 5998 (1990).
[7] U. Schneider, M. de la Torre Juarez, W. Zimmermann, and I. Rehberg, Phys. Rev. A **46**, 1009 (1992).
[8] S. Kai and K. Hirakawa, Suppl. Prog. Theor. Phys. **64**, 212 (1978).
[9] A. Joets and R. Ribotta, Phys. Rev. Lett. **60**, 2164 (1988).
[10] I. Rehberg, S. Rasenat, and V. Steinberg, Phys. Rev. Lett. **62**, 756 (1989).
[11] M. Dennin, D. S. Cannell, and G. Ahlers, Mol. Cryst. Liq. Cryst. Sci. Technol., Sect. A **261**, 337 (1995).
[12] M. Treiber and L. Kramer, Mol. Cryst. Liq. Cryst. Sci. Technol., Sect. A **261**, 311 (1995).
[13] M. Dennin, M. Treiber, L. Kramer, G. Ahlers, and D. S. Cannell, Phys. Rev. Lett. **76**, 319 (1996).
[14] M. Treiber, N. Éber, Á. Buka, and L. Kramer, J. Phys. II **7**, 649 (1997).
[15] Á. Buka, B. Dressel, W. Otowski, K. Camara, T. Tóth-Katona, L. Kramer, J. Lindau, G. Pelzl, and W. Pesch, Phys. Rev. E **66**, 051713 (2002); Á. Buka, B. Dressel, L. Kramer, and W. Pesch, Phys. Rev. Lett. **93**, 044502 (2004); Chaos **14**, 793 (2004).
[16] S. Kai, K. Hayashi, and Y. Hidaka, J. Phys. Chem. **100**, 19007 (1996).
[17] Á. Buka, P. Toth, N. Éber, and L. Kramer, Phys. Rep. **337**, 649 (2000).
[18] Á. Buka, N. Éber, W. Pesch, and L. Kramer, in *Self Assembly, Pattern Formation and Growth Phenomena in Nano-Systems*, edited by A. A. Golovin and A. A. Nepomnyaschy (Springer, New York, 2006), p. 55.
[19] M. Goscianski and L. Léger, J. Phys. (France) **36**, 231 (1975).
[20] L. M. Blinov, M. I. Barnik, V. T. Lazareva, and A. N. Trufanov, J. Phys. (France) **40**, 263 (1979).
[21] E. Kochowska, S. Németh, G. Pelzl, and Á. Buka, Phys. Rev. E **70**, 011711 (2004).
[22] M. I. Barnik, L. M. Blinov, S. A. Pikin, and A. N. Trufanov, Sov. Phys. JETP **45**, 396 (1977).
[23] N. V. Madhusudana and V. A. Raghunathan, Mol. Cryst. Liq. Cryst. **56**, 201 (1988); Liq. Cryst. **5**, 1789 (1989).
[24] H. Kresse, A. Wiegeleben, and D. Demus, Krist. Tech. **15**, 341 (1980).
[25] M. Goscianski, Philips Res. Rep. **30**, 37 (1975).
[26] Surprisingly, in **8/7** we do see both ns-EC, and at high temperatures *s*-EC in a thin (d=3.4 μm) cell at higher frequencies. Even more surprising is the frequency dependence of the threshold showing an expressed minimum. ns-EC sets in at $f \approx 100$ Hz at a relatively high threshold ($U_c \approx 40$ V). With the

increase of f, U_c rapidly falls and reaches a minimum of $U_c \approx 10-15$ V at $f \approx 300$ Hz and then grows again. Above $f \approx 500$Hz, the dependence of U_c on f is linear, similarly to the case in thicker cells shown, e.g., in Fig. 3. Detailed analysis of the phenomena is in progress. Unfortunately, however, one cannot compare these results directly with those obtained in thicker cells, as there the ns-EC— if it exists at all at these high frequencies—would have such an extremely high threshold that would cause dielectric breakdown of the samples.

[27] E. Dubois-Violette, P. G. de Gennes, and O. Parodi, J. Phys. (Paris) **32**, 305 (1971).

[28] J.-H. Huh, Y. Yusuf, Y. Hidaka, and S. Kai, Phys. Rev. E **66**, 031705 (2002).

[29] R. Ribotta and G. Durand, J. Phys. (France) **40**, 334 (1979).

[30] L. K. Vistin, Kristallografiya **15**, 594 (1970).

[31] W. Greubel and U. Wolff, Appl. Phys. Lett. **19**, 213 (1971).

[32] Yu. P. Bobylev and S. A. Pikin, Sov. Phys. JETP **45**, 195 (1977).

[33] W. Pesch and A. P. Krekhov (private communication).

[34] T. Tóth-Katona, N. Éber, and Á. Buka (unpublished).

[35] W. Decker, Diploma work, University of Bayreuth, 1990.